Nanostructured Hybrid Transparent Conductive Films with Antibacterial Properties

Iskandar N. Kholmanov,[†,‡] Meryl D. Stoller,[†] Jonathan Edgeworth,[†] Wi Hyoung Lee,[†] Huifeng Li,[†] Jongho Lee,[§] Craig Barnhart,[⊥] Jeffrey R. Potts,[†] Richard Piner,[†] Deji Akinwande,[§] Jeffrey E. Barrick,[⊥] and Rodney S. Ruoff[†,*]

[†]Department of Mechanical Engineering and Materials Science and Engineering Program, The University of Texas at Austin, 1 University Station C2200, Austin, Texas 78712, United States, [‡]CNR-IDASC Sensor Lab Department of Chemistry and Physics, University of Brescia, Via Valotti, 9, Brescia 25133, Italy, [§]Microelectronic Research Center, Department of Electrical Engineering and The University of Texas at Austin, Austin, Texas 78758, United States, and [⊥]Chemistry and Biochemistry, Institute for Cellular and Molecular Biology, The University of Texas at Austin, Austin, Texas 78712, United States

ABSTRACT Here, we demonstrate that the assembly of nanostructures with different dimensionalities yields "multicomponent hybrid" transparent conductive films (TCFs) with sheet resistance and optical transmittance comparable to that of indium tin oxide (ITO) films. It was shown that sheet resistance of single-component Ag nanowire (NW) films can be further decreased by introducing gold-decorated reduced graphene oxide (RG-O) nanoplatelets that bridge the closely located noncontacting metal NWs. RG-O nanoplatelets can act as a protective and adhesive layer for underneath metal NWs, resulting in better performance of hybrid TCFs compared to single-component TCFs. Additionally, these hybrid TCFs possess antibacterial properties, demonstrating their multifunctional characteristics that might have a potential for biomedical device applications. Further development of this strategy paves a way toward next generation TCFs composed of different nanostructures and characterized by multiple (or additional) functionalities.

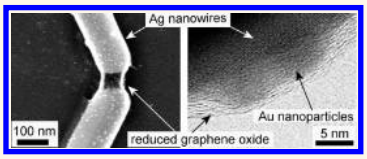

KEYWORDS: transparent conducive films · reduced graphene oxide · nanowires · hybrid films · antibacterial films

Today, indium tin oxide (ITO) is the main material used for transparent conductive films (TCFs). However, the brittle ceramic structure, poor compatibility with organic materials, and the growing cost of indium seriously limit the use of ITO in TCFs, especially in emerging flexible electronics and large-area applications.[1−7] Therefore, several other materials including new oxide films,[2,8] conductive polymers,[9] carbon nanotubes (CNTs),[10,11] metal nanostructures,[12−15] and graphene-based nanostructures[16−21] have been investigated as alternatives to ITO. Among these materials, one-dimensional (1D) CNTs and metal nanowires (NWs) and 2D graphene-based films are particularly interesting due to their good TCF characteristics, such as low sheet resistance (R_s) and high optical transmittance (T), which are comparable to/or better than that of ITO films. However, their use in a wide range of TCF-using devices is restricted by several specific drawbacks. Metal NW and CNT films are characterized by open spaces between nanostructures, high surface roughness, and poor adhesion to substrates. In addition, the high reactivity of metal NW films may cause oxidation that can limit their long-term applications. In contrast, 2D graphene films grown by chemical vapor deposition (CVD) of hydrocarbon gases[22] are characterized by continuous film morphology and excellent TCF characteristics (R_s = 30 Ω/sq with optical transmittance of 90% at 550 nm wavelength (T_{550})).[17] Drawbacks of graphene films include the currently costly fabrication procedures that use vacuum and high temperature and the time-consuming and challenging multiple transfer steps from metal to the transparent substrate. Moreover, the growth of functional films with controlled morphology on graphene might be challenging due to the low density of nucleation sites on CVD-grown graphene and, therefore, may require further treatments.[23] These disadvantages are absent in reduced graphene oxide (RG-O) films, which are another candidate for TCF applications.[18,24] RG-O films are obtained by simple solution processing, allowing direct deposition on any substrate. The main drawback of RG-O films is the relatively high R_s (>1 kΩ/sq at T_{550} > 85%).[18,24]

These shortcomings of single-component TCFs might be overcome by hybrid films, in which the film properties can be improved due to synergy between individual components.[25−27] Zhu *et al.* reported the better performance (R_s = 20 Ω/sq at T_{550} = 90%) of graphene/metal grid hybrid

* Address correspondence to r.ruoff@mail.utexas.edu.

Received for review February 25, 2012 and accepted April 22, 2012.

Published online April 22, 2012
10.1021/nn300852f

systems compared to corresponding single-component TCFs.[26] Recent theoretical studies of graphene/metal NW TCFs demonstrate a promising approach to decrease the sheet resistance of graphene using metal NWs.[27] Moreover, hybrid TCFs may exhibit additional functionalities that can vary depending on their composition. This feature opens up possibilities for developing next generation multicomponent and multifunctional TCFs.

Here, we demonstrate a general strategy for assembling TCFs composed of zero-dimensional (0D) Au nanoparticles (NPs), 1D Ag nanowires (NWs), and 2D RG-O platelets. The decreased sheet resistance of the hybrid films, compared to the single-component films, has been demonstrated both macroscopically by measuring the sheet resistance of 1×1 cm^2 area films and microscopically by measuring the resistance between two parallel noncontacting Ag NWs bridged by RG-O coverage. Performance of other thin film characteristics and additional functionality of the hybrid films have been shown to demonstrate the advantage of the hybrid films.

RESULTS AND DISCUSSION

Among RG-O platelets, Au NPs, and Ag NWs, the Ag NWs and RG-O platelets can form single-component TCFs. Figure 1a shows the TCF characteristics of Ag NW films obtained by spin coating of NW dispersions in isopropyl alcohol with three different concentrations: 1.0, 2.0, and 2.5 mg/mL on glass substrates. The average length and diameter of the NWs are in the range of 20−40 μm and 100−130 nm, respectively (see Supporting Information). High optical transparency of the Ag NW TCFs is provided by the open spaces between nanowires and decreases with increasing NW concentration in the film. The Ag NW films, obtained using the 1.0 mg/mL dispersion, are nonconductive because of subpercolation networks of NWs and possess T_{550} = 96% (Figure 1a). Electrical conductivity of the films, obtained using 2.0 and 2.5 mg/mL dispersions, is provided through the percolation network between nanowires,[28] resulting in R_s of 740 ± 34 and 520 ± 23 Ω/sq for T_{550} of 90 and 88%, respectively (Figure 1a).

The main contribution to the overall resistance of the NW films might be expected to be from the junctions formed by crossing NWs. In our films, the measured NW−NW junction resistances (61 and 67 Ω) are very close to the resistance of individual NWs (61 and 77 Ω), demonstrating good contact between crossed Ag NWs (Figure 1b; see also Supporting Information).

In contrast to the Ag NW films, RG-O films are continuous and smooth. A typical RG-O film with R_s = 49.2 ± 4.47 kΩ/sq possesses $T_{550} \approx$ 94% (Figure 1c). Such high R_s values can be ascribed to the presence of defects[29] introduced during the synthesis and processing of G-O and interlayer resistance between the RG-O platelets. In an attempt to minimize and/or eliminate the role of the two factors, we combined Au NPs and Ag NWs with RG-O platelets to create hybrid films. Our concept is based on a strategy in which each component improves the hybrid film by addressing the weaknesses of the other components.

Adding Au NPs significantly decreases the resistance of the RG-O platelets (Figure 1c), likely due to the NPs decorating defect sites.[30] R_s values of RG-O/Au NP films (28.6 ± 1.43 kΩ/sq), obtained using a 0.5 mg/mL G-O dispersion, were significantly lower than that for the corresponding RG-O films (49.2 ± 4.47 kΩ/sq). The Au NPs do not influence the T values of the RG-O/Au NP films (Figure 1c), probably because of their low concentration and small size (see Supporting Information).

Ag NWs were added with the goal of minimizing and/or eliminating the junction resistance between RG-O platelets. Fabrication of the hybrid RG-O/Au NP/Ag NW TCFs, composed of a film of Ag NWs covered by a RG-O/Au NP film, is shown schematically in Figure 2a. Hybrid films with R_s = 26 ± 1.04 Ω/sq at T_{550} = 83% (Figure 2b), comparable to ITO ($R_s \approx$ 30 Ω/sq at $T_{550} \approx$ 90%), were obtained. This architecture allowed us to obtain conductive hybrid films that even have a subpercolation (nonconductive) Ag NW film, demonstrating the synergy of the various components (Figure 2c).

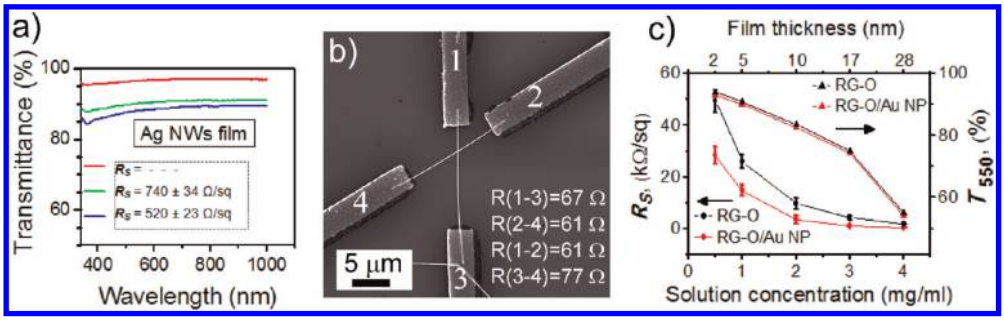

Figure 1. (a) R_s and T of Ag NW films obtained using three different concentrations of the Ag NW dispersions: (red) 1.0 mg/mL, (green) 2.0 mg/mL, and (blue) 2.5 mg/mL. (b) SEM image of a NW−NW junction with four Ni electrodes used to measure the resistance of individual NWs and the junction resistance between NWs. (c) R_s and T of RG-O and RG-O/Au NP films obtained by spin coating of the G-O and G-O/Au NP dispersions with different concentrations and then exposing the films to hydrazine vapor at 100 °C.

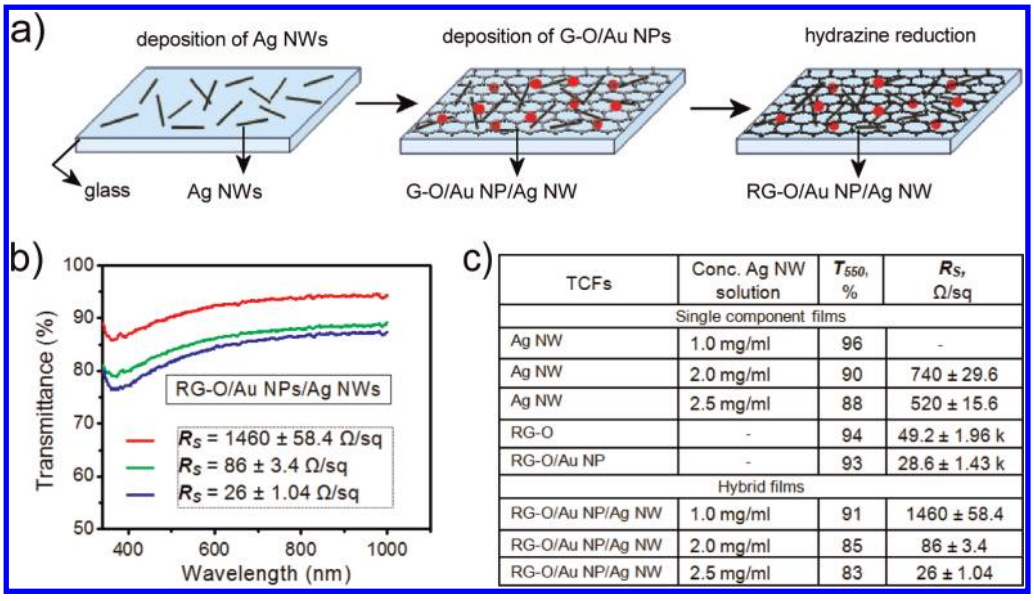

TCFs	Conc. Ag NW solution	T_{550}, %	R_S, Ω/sq
Single component films			
Ag NW	1.0 mg/ml	96	-
Ag NW	2.0 mg/ml	90	740 ± 29.6
Ag NW	2.5 mg/ml	88	520 ± 15.6
RG-O	-	94	49.2 ± 1.96 k
RG-O/Au NP	-	93	28.6 ± 1.43 k
Hybrid films			
RG-O/Au NP/Ag NW	1.0 mg/ml	91	1460 ± 58.4
RG-O/Au NP/Ag NW	2.0 mg/ml	85	86 ± 3.4
RG-O/Au NP/Ag NW	2.5 mg/ml	83	26 ± 1.04

Figure 2. (a) Schematic of hybrid film preparation. Ag NWs were spin coated on glass slides. The resulting NW film was then covered with a G-O/Au NP (0.5 mg/mL) film by spin coating, and the final hybrid film was exposed to hydrazine vapor at 100 °C for 24 h. (b) Optical transmittance spectra and R_s of the hybrid films obtained using three different concentrations of the Ag NW dispersions: (red) 1.0 mg/mL, (green) 2.0 mg/mL, and (blue) 2.5 mg/mL. (c) R_s and T_{550} data for single-component and hybrid films.

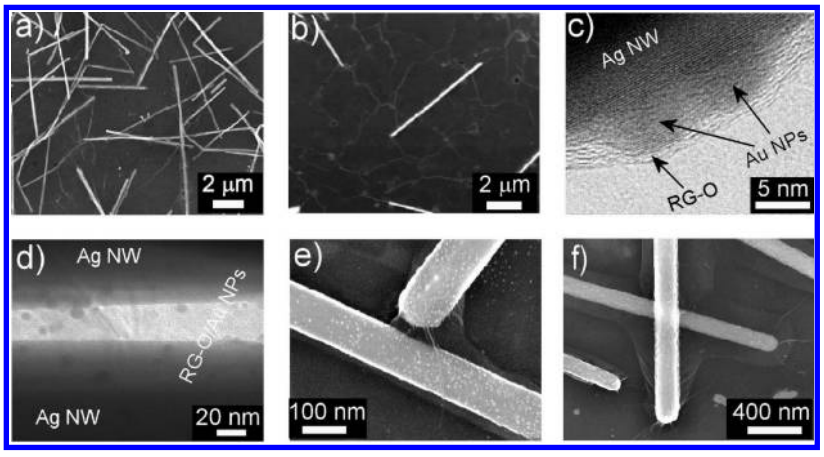

Figure 3. (a) Typical SEM image of the hybrid films composed of Ag NWs covered by a RG-O/Au NPs film (see also Figure S3 in Supporting Information). (b) Ag NW connecting several RG-O/Au NP platelets. (c) TEM image of the RG-O/Au NP/Ag NW film showing individual components contacting each other. (d) TEM image of RG-O/Au NP film bridging two parallel Ag NWs. (e) SEM image of noncontacting Ag NWs bridged by the RG-O/Au NP film. (f) RG-O/Au NP film covering the entire surface including all Ag NWs, some of which are resting on the substrate with another stacked upon the others.

Structural analysis of the hybrid films suggests some details of the role of each component in improving the performance of the hybrid films. Typical SEM images show hybrid films composed of randomly oriented Ag NWs covered by the RG-O/Au NPs film (Figure 3a). Ag NWs possessing the highest electrical conductivity among the single components can connect two or more RG-O platelets, decreasing the interplatelet resistance (Figure 3b). Au NPs can be located either between RG-O and Ag NWs where all three components tightly contact each other (Figure 3c) or trapped on RG-O platelets serving as a bridge between NWs (Figure 3d). SEM images shown in Figure 3e,f indicate some important features of the 2D RG-O platelets that can contribute to the performance of the hybrid films. Particularly, RG-O platelets cover almost half of the surface of a typical Ag NW by following its curvature (Figure 3e), providing a high contact area between RG-O and NWs that enhances charge transfer between these two nanostructures and improves conductivity. In addition, a certain number of NWs do not directly contact the substrate because they lay across the top of other NWs that directly contact the substrate (Figure 3f). The RG-O/Au NP film covers the entire surface, including all NWs and open spaces between NWs. The latter is particularly important, for instance, for applications in photovoltaic devices since the charge

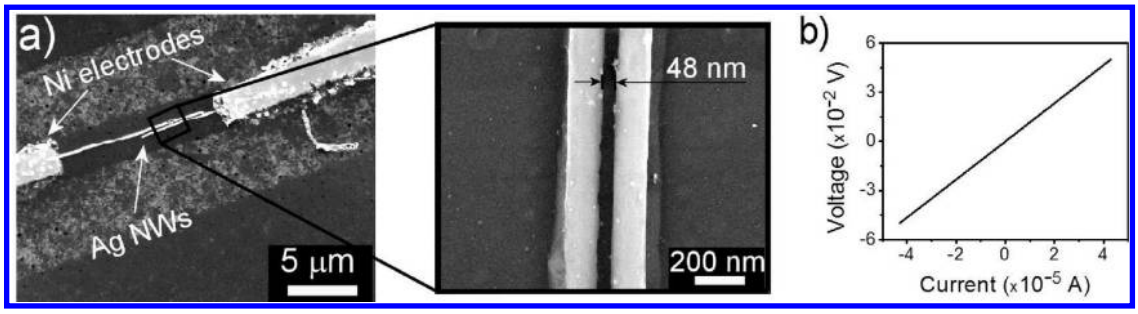

Figure 4. (a) SEM images of two parallel NWs, individually contacted with Ni electrodes and covered with a RG-O/Au NP film, used to measure the resistance of the system. Inset shows a higher magnification image showing the distance of 48 nm between the parallel Ag NWs (see also Figure S4 in Supporting Information). (b) *I*−*V* characteristic of the system.

diffusion distance in hybrid films is smaller compared with the spacing between NWs.

The RG-O platelets can reduce the R_s of the NW film by bridging noncontacting NWs. This is particularly pronounced between nearby NWs. Figure 4a shows two parallel NWs covered with the RG-O/Au NP film (see also Supporting Information). Without the RG-O/Au NP film, the system was not conducting. Once the RG-O/Au NP film was added, the NWs became connected with a resistance of 1.16 kΩ, showing that the RG-O/Au NP film acts as a 2D bridge between NWs to provide good electrical conductivity. Linear *I*−*V* characteristic indicates the formation of ohmic contacts between parallel NWs and RG-O film (Figure 4b).

It should be noted that, on one hand, R_s values of our pure Ag NWs films are higher compared to those in the recently reported papers.[31,32] On the other hand, the junction resistance between crossed NWs is much lower than reported by Hu *et al.*[12] Such differences are likely due to the difference in precursor materials and/or experimental conditions used to produce the NW films. The importance of our results is that by using 2D RG-O platelets the sheet resistance of 1D NW films can be further decreased, as shown both by macroscopic measurements of the R_s values (Figure 2c) and by microscopic studies of two parallel NWs covered with RG-O platelets (Figure 4). Thus, using our approach for Ag NW TCFs with better TCF characteristics, one can obtain higher performance hybrid TCFs.

Although all of the films presented in this work were on rigid inflexible substrates, one might expect similar results for flexible substrates because (i) all thin film fabrication and processing have been performed at temperatures compatible with processing of flexible substrates, and (ii) single-component TCFs of RG-O and of Ag NWs on flexible substrates have already been demonstrated.[14,18]

Thus, the assembly of these 0D, 1D, and 2D nanostructures allows one to obtain hybrid films, where the weaknesses of each component are offset by the strengths of the other components. The overall composition and architecture (RG-O/Au NPs on top of NWs) not only results in higher conductivity but also provides better performance. In particular, the RG-O film might act as a protective layer for the metal NWs underneath from possible oxidation or corrosion processes and may provide a more continuous network.

Another distinguishable feature of hybrid TCFs might be their multifunctionality arising due to either the individual functionality of each single component or integrative synergy between single constituents. Such additional functionality of our hybrid films may be their bactericidal activity since both silver nanostructures[33] and recently RG-O platelets[34,35] have been shown to be toxic to diverse bacteria. Taking this fact into account, we investigated the antibacterial properties of the RG-O/Au NP/Ag NW hybrid films against *Escherichia coli* bacteria by carrying out two types of experiments. We first investigated the ability of bacteria to attach to hybrid films in solution in adhesion experiments. We then studied the growth of bacterial colonies from solutions sprayed on the hybrid film surfaces in viability experiments.

In the adhesion experiments, two Si wafers, one coated with the hybrid film and one without, were submerged in separate, but identical, bacterial solutions and incubated overnight. The samples were then removed from the bacterial solution and delicately washed with distilled water to remove excess bacterial solution. A typical SEM image of a clean Si wafer after this treatment (Figure 5a) shows a large number of *E. coli* bacteria attached to its surface. The size of a typical bacterium attached to the wafer is about 2 μm in length and 1 μm in width, as shown in the SEM image in the Figure 5a inset. In contrast to the clean Si wafers, on the hybrid film-covered Si wafers (Figure 5b), after this treatment, one can observe a few black objects with sizes ranging from tens to hundreds of nanometers. These objects are significantly smaller than intact *E. coli* bacterium size (Figure 5a inset). We suggest that these objects are the remains of *E. coli* disrupted by interacting with the hybrid film. In contact with the RG-O platelets, the outer membrane of the bacteria can be damaged,[34] resulting in a loss of cellular integrity. Therefore, the observed results, where no intact bacteria adhere to the hybrid films (Figure 5b), can likely be ascribed to these bactericidal properties.

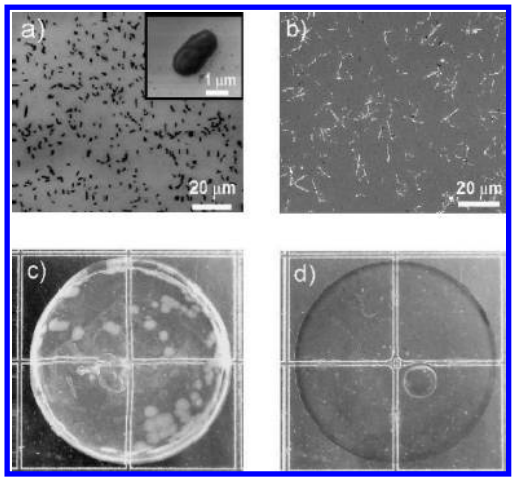

Figure 5. Antibacterial properties of the RG-O/Au NP/Ag NW hybrid TCF films: SEM images of (a) clean Si wafer and (b) Si wafer covered with a RG-O/Au NP/Ag NW hybrid film (white streaks are the Ag NWs obtained using a 1.0 mg/mL Ag NW dispersion) after the adhesion experiments. A typical E. coli bacterium is shown in the inset of panel a. Photographs of (c) clean glass slide and (d) glass slide covered with RG-O/Au NP/Ag NW hybrid films after the viability experiments. White areas in (c) correspond to bacterial colonies grown during incubation.

It is worth noting that after this experiment the TCF characteristics of the hybrid films can be easily recovered by annealing the films at 100 °C for 30 min under ambient atmosphere. In contrast, pure Ag NW films left overnight in the bacterial solution irreversibly lost their TCF characteristics because most of the Ag NWs were detached from the substrate. These results demonstrate an essential advantage of the hybrid TCFs over pure Ag NW TCFs and show that the presence of the top RG-O coverage promotes adhesion of all components of the hybrid films to the substrate, even in liquid solutions. In this context, pure Ag NW TCFs have serious limitations in use in solution-based treatment and growth processes and cannot be applied, for instance, in widely used solution-based electrochemical growth of functional films on top of TCFs.

In the viability experiments, an overnight culture of *E. coli* bacteria solution was sprayed onto the surface of two glass slides, one with and one without the hybrid film. After drying for about 3 min, both slides were covered with an agar solution and incubated overnight. Bacteria sprayed on the clean glass slide formed bacterial colonies (white dots in Figure 5c). An average of 34 colonies/slide (averaged over 11 tested samples) was observed. No bacterial colonies were observed on the hybrid film-covered glass slides (Figure 5d). These results show that the spray-deposited bacteria on top of the hybrid films were completely inactivated, indicating the toxicity of the hybrid films to *E. coli* bacteria.

The antibacterial properties of the hybrid films demonstrated in these two different types of experiments can be ascribed mainly to the RG-O since it is the top layer and in direct contact with the bacteria. Indeed, pure RG-O films with no NWs provided similar antibacterial results (see Figure S5 in Supporting Information). The mechanism of the microbial activity of the RG-O films can be described by taking into account both membrane and oxidative stresses.[34] The membrane stress is caused by direct contact of the bacteria with sharp edges of the RG-O platelets disrupting the outer membrane of the cells and causing subsequent oxidative stresses. In addition, it was reported that antibacterial activity of conductive RG-O differs from that of electrically insulating G-O platelets, and this can be ascribed to the difference in charge transfer processes in bacteria/RG-O and bacteria/G-O systems.[35] In this context, combination of the TCF characteristics with the antibacterial properties may allow producing hybrid TCFs with controlled bioactivity. In particular, charge transfer processes between the bacteria and RG-O in the hybrid TCFs can be tuned by applying external electrical and/or optical fields.

Thus, assembly of the antibacterial RG-O platelets with highly conductive Ag NW films yields hybrid TCFs with improved electrical conductivity and bactericidal properties. Antibacterial hybrid TCFs with integrated functionalities can be used as bactericidal and transparent electromagnetic interference (EMI) shielding coatings. This application might be attractive, for instance, for displays and windows of diverse medical electronics, such as medical computers and magnetic resonant imaging windows, and also for personal electronics such as cell phones, media players, and computers for which healthcare issue is of importance. This application aspect is strengthened by the fact that silver[36] and carbon nanostructures[37,38] including transparent conductive CNT films[39] possess highly effective EMI shielding characteristics. In these applications, the antibacterial hybrid TCFs provide electrically conductive, optically transparent, and medically clean sterile environments. Further investigations of the correlation between electro-optical properties and antibacterial characteristics, which are currently in progress, will give a better understanding of the interactions of graphene-based materials with microorganisms and might open a way toward developing innovative biomedical applications for multifunctional hybrid TCFs.

CONCLUSION

Thus, our approach demonstrates that covering the highly conductive metal NW-based TCFs with 2D Au-decorated RG-O platelets has vital practical importance to yield better TCF characteristics due to the synergy between the nanostructures used, with the additional benefit of providing antibacterial activity. Two-dimensional RG-O platelets can act as a protective and adhesive layer, conductive bridge to the non-directly contacting metal NWs, and also provide a more continuous network, which is important for

applications in photovoltaic devices since the charge diffusion distance is smaller compared with the spacing between NWs. The presented strategy based on the use of 0D, 1D, and 2D nanostructures offers exciting possibilities for generating multifunctional TCFs with novel architectures. For example, the Au NPs could be replaced by semiconductor quantum dots, or plasmonic or catalytic NPs, and the Ag NWs could be replaced by other 1D nanostructures with different optical, magnetic, electronic, and catalytic responses. Such hybrid TCFs might improve the performance of existing and emerging devices.

METHODS

Synthesis of Nanostructures Used To Fabricate Hybrid Films. Graphite oxide was produced from natural graphite (SP-1, Bay Carbon, MI) using a modified version of the Hummers method, as detailed previously.[40] Aqueous dispersions of individual graphene oxide (G-O) platelets of the various concentrations were prepared by stirring graphite oxide solids in pure water (17.5 MΩ, Barnstead) for 3 h, and then sonicating the mixture (VWR B2500A-MT, a bath sonicator) for 45 min.

Aqueous solutions of Au NPs were prepared through the addition of 0.01 g of sodium borohydride ($NaBH_4$) to 100 mL of an aqueous solution (10^{-4} M) of tetrachloroauric acid ($HAuCl_4$) at room temperature, as detailed elsewhere.[41] The G-O/Au NP dispersions were formed by combining freshly prepared Au NP solutions with G-O dispersions of various concentrations in 1:1 volume ratios.

Ag NWs with average length of 20−40 μm and average diameter of 100−130 nm (Figure S1) dispersed in isopropyl alcohol (20 mg/mL) were purchased from SeaShell Technology. The initial solution was diluted with isopropyl alcohol (99.9%, Fisher Scientific) in order to obtain 1.0, 2.0, and 2.5 mg/mL concentrated Ag NW dispersions.

Thin Film Fabrication and Characterization. Glass slides and Si wafers (with a 280 nm thick oxide layer) were used as substrates and were first cleaned with piranha solution (concentrated H_2SO_4 and 30% H_2O_2 solution mixed at a 3:1 volumetric ratio) at 120 °C for 25 min, carefully rinsed with DI water several times, then immediately used for film deposition. G-O, Ag NW, and G-O/Au NP films were obtained by spin coating (4000 rpm) of the corresponding dispersions. G-O/Ag NW and Au NP/Ag NW films were produced by two sequential spin coating processes, each time using a dispersion of the corresponding single components. G-O/Au NP/Ag NW films were deposited as schematically shown in Figure 2a. All G-O-containing films were subsequently reduced through exposure to N_2H_4 (hydrazine monohydrate, 98%, Sigma Aldrich) vapor at 100 °C for 24 h. Scanning electron microscopy (SEM) (Hitachi S-5500 SEM equipped with STEM) and transmission electron microscopy (TEM) (JEOL 2010F TEM, and using Quantafoil copper TEM grids from Ted Pella Inc.) were used to characterize the structural properties of the nanostructures and thin films. Optical transmittance (T) of the films was measured using UV−vis−NIR spectroscopy (Cary 5000) and spectroscopic ellipsometry (J.A. Wollam M2000). The latter was used to measure the film thickness, as well. To measure the sheet resistance (R_s) using the four-probe van der Pauw method, four gold electrodes were deposited on the film in a configuration that leaves squared film area with a size in the range of 1×1 cm^2.

Antibacterial Material Synthesis and Characterization. The bacterial strain used was *Escherichia coli* B REL 606 (Gram-negative). Luria−Bertani (LB) broth used for growth contained (per liter of deionized water) 10 g of tryptone, 5 g of yeast extract, and 10 g of NaCl. This solution was autoclaved for 30 min prior to use. For both types of experiments, the *E. coli* were prepared as follows: a small amount of frozen *E. coli* was transferred from a −80 °C glycerol stock into 10 mL of LB media in a glass culture tube, followed by shaking at 120 rpm and 37 °C for 24 h (Innova 44 Incubator Shaker, New Brunswick Scientific). Following the 24 h incubation period, the tubes contained approximately 2×10^9 CFU (colony forming units) mL^{-1} of *E. coli*. For the adhesion experiments (Figure 5a,b), two cultures of *E. coli* were prepared as above. Following the 24 h incubation period, all 10 mL of each bacterial culture was transferred in sterile conditions into a 50 mL conical tube. The Si substrates (with 280 nm SiO_2 oxide layer), with and without the hybrid films, were then put into separate conical tubes and incubated for another 24 h at 37 °C with no shaking (Precision Model 815 Incubator, Thermo Scientific). Overall, 18 samples (9 clean Si wafers and 9 Si wafer covered with the hybrid films) have been tested in three separate runs of the adhesion experiment. Typical SEM images of the samples after the adhesion experiments are shown in Figure 5a,b. For the viability experiments, the bacteria, following the 24 h incubation period, were transferred in sterile conditions into a glass bottle that was attached to a sprayer (Preval spray unit, Sigma-Aldrich). The bacteria were then sprayed onto glass slides (circle shape VWR micro-cover glass with a diameter of 18 mm), with and without the hybrid films (number of sprays: 2−3 times, until the surface was almost fully covered by liquid droplets). The glass slides were air-dried for 3 min then completely covered with a melted agar (0.8% w/v) LB solution that was allowed to solidify at room temperature before incubating overnight at 37 °C to allow viable cells to form colonies. Overall, 21 samples (11 clean glass slides and 10 glass slides covered with the hybrid films) have been tested in four separate runs of the viability experiment. The photographs shown in Figure 5c,d have been taken with rear white-light illumination on a colony counter (Galaxy 230 colony counter, Rocker).

Conflict of Interest: The authors declare no competing financial interest.

Acknowledgment. This work was supported by a Tokyo Electron Ltd. (TEL)-customized Semiconductor Research Corporation award (Project #2009-OJ-1873−development of graphene-based transparent conductive films for display applications).

Supporting Information Available: Synthesis and characterization of two-component hybrid films, details of fabrication and electrical conductivity of individual crossed Ag NWs and RG-O/Au NP covered parallel Ag NWs and additional information on antibacterial properties of the hybrid films. This material is available free of charge *via* the Internet at http://pubs.acs.org.

REFERENCES AND NOTES

1. van de Lagemaat, J.; Barnes, T. M.; Rumbles, G.; Shaheen, S. E.; Coutts, T. J.; Weeks, C.; Levitsky, I.; Peltola, J.; Glatkowski, P. Organic Solar Cells with Carbon Nanotubes Replacing In_2O_3:Sn as the Transparent Electrode. *Appl. Phys. Lett.* **2006**, *88*, 233503(1−3).
2. Liang, H.; Roy, G. Atmospheric Pressure Chemical Vapor Deposition of Transparent Conducting Films of Fluorine Doped Zinc Oxide and Their Application to Amorphous Silicon Solar Cells. *J. Mater. Sci.* **2007**, *42*, 6388–6399.
3. Ju, S.; Facchetti, A.; Xuan, Y.; Liu, J.; Ishikawa, F.; Ye, P.; Zhou, C.; Marks, T. J.; Janes, D. B. Fabrication of Fully Transparent Nanowire Transistors for Transparent and Flexible Electronics. *Nat. Nanotechnol.* **2007**, *2*, 378–384.
4. Sekitani, T.; Nakajima, H.; Maeda, H.; Fukushima, T.; Aida, T.; Hata, K.; Someya, T. Stretchable Active-Matrix Organic Light-Emitting Diode Display Using Printable Elastic Conductors. *Nat. Mater.* **2009**, *8*, 494–499.

5. Lipomi, D. J.; Vosgueritchian, M.; Tee, B. C.-K.; Hellstrom, S. L.; Lee, J. A.; Fox, C. H.; Bao, Z. Skin-like Pressure and Strain Sensors Based on Transparent Elastic Films of Carbon Nanotubes. *Nat. Nanotechnol.* **2011**, *6*, 788–792.
6. Yang, Y.; Jeong, S.; Hu, L.; Wu, H.; Lee, S. W.; Cui, Y. Transparent Lithium-Ion Batteries. *Proc. Natl. Acad. Sci. U.S.A.* **2011**, *108*, 13013–13018.
7. De Jong, M. P.; Simons, D. P. L; Reijme, M. A.; IJzendoorn, L. J.; Gon, A. W. D.; Voigt, M. J. A.; Brongersma, H. H.; Gymer, R. W. Indium Diffusion in Model Polymer Light-Emitting Diodes. *Synth. Met.* **2000**, *110*, 1–6.
8. Mizoguchi, H.; Kamiya, T.; Matsuishi, S.; Hosono, H. A Germanate Transparent Conductive Oxide. *Nat. Commun.* **2011**, *470*, DOI: 10.1038/ncomms1484.
9. Burroughes, J. H.; Bradley, D. D. C.; Brown, A. R.; Marks, R. N.; Mackay, K.; Friend, R. H.; Burns, P. L.; Holmes, A. B. Light-Emitting Diodes Based on Conjugated Polymers. *Nature* **1990**, *347*, 539–541.
10. Wu, Z.; Chen, Z.; Du, X.; Logan, M. J.; Sippel, J.; Nikolou, M.; Karamas, K.; Reynolds, J. R.; Tanner, D. B.; Hebard, A. F.; *et al.* Transparent, Conductive Carbon Nanotube Films. *Science* **2004**, *305*, 1273–1276.
11. Shim, B. S.; Zhu, J. A.; Jan, E.; Critchley, K.; Kotov, N. A. Transparent Conductors from Layer-by-Layer Assembled SWNT Films: Importance of Mechanical Properties and a New Figure of Merit. *ACS Nano* **2010**, *4*, 3725–3734.
12. Hu, L.; Kim, H. S.; Lee, J. Y.; Peumans, P.; Cui, Y. Scalable Coating and Properties of Transparent, Flexible, Silver Nanowire Electrodes. *ACS Nano* **2010**, *4*, 2955–2963.
13. Rathmell, A. R.; Wiley, B. J. The Synthesis and Coating of Long, Thin Copper Nanowires To Make Flexible, Transparent Conducting Films on Plastic Substrates. *Adv. Mater.* **2011**, *23*, 4798–4803.
14. Azulai, D.; Belenkova, T.; Gilon, H.; Barkay, Z.; Markovich, G. Transparent Metal Nanowire Thin Films Prepared in Mesostructured Templates. *Nano Lett.* **2009**, *9*, 4246–4249.
15. Wu, H.; Hu, L.; Rowell, M. W.; Kong, D.; Cha, J. J.; McDonough, J. R.; Zhu, J.; Yang, Y.; McGehee, M. D.; Cui, Y. Electrospun Metal Nanofiber Webs as High-Performance Transparent Electrode. *Nano Lett.* **2010**, *10*, 4242–4248.
16. Li, X.; Zhu, Y.; Cai, W.; Borysiak, M.; Han, B.; Chen, D.; Piner, R. D.; Colombo, L.; Ruoff, R. S. Transfer of Large-Area Graphene Films for High-Performance Transparent Conductive Electrodes. *Nano Lett.* **2009**, *9*, 4359–4363.
17. Bae, S.; Kim, H. K.; Lee, Y.; Xu, X.; Park, J. S.; Zheng, Y.; Balakrishnan, J.; Im, D.; Lei, T.; Song, Y. I.; *et al.* Roll-to-Roll Production of 30-in. Graphene Films for Transparent Electrodes. *Nat. Nanotechnol.* **2010**, *5*, 574–578.
18. Yamaguchi, H.; Eda, G.; Mattevi, C.; Kim, H. K.; Chhowalla, M. Highly Uniform 300 mm Wafer Scale Deposition of Single and Multilayered Chemically Derived Graphene Thin Films. *ACS Nano* **2010**, *4*, 524–528.
19. Kang, J.; Kim, H.; Kim, K. S.; Lee, S. K.; Bae, S.; Ahn, J. H.; Kim, Y. J.; Choi, J. B.; Hong, B. H. High-Performance Graphene-Based Transparent Flexible Heaters. *Nano Lett.* **2011**, *11*, 5154–5158.
20. Pang, S.; Hernandez, Y.; Feng, X.; Müllen, K. Graphene as Transparent Electrode Material for Organic Electronics. *Adv. Mater.* **2011**, *23*, 2779–2795.
21. Lee, J. M.; Choung, J. W.; Yi, J.; Lee, D. H.; Samal, M.; Yi, D. K.; Lee, C. H.; Yi, G. C.; Paik, U.; Rogers, J. A. Vertical Pillar-Superlattice Array and Graphene Hybrid Light Emitting Diodes. *Nano Lett.* **2010**, *10*, 2783–2788.
22. Li, X.; Cai, W.; An, J.; Kim, S.; Nah, J.; Yang, D.; Piner, R.; Velamakanni, A.; Jung, I.; Tutuc, E.; *et al.* Large-Area Synthesis of High-Quality and Uniform Graphene Films on Copper Foils. *Science* **2009**, *324*, 1312–1314.
23. Chung, K.; Lee, C. H.; Yi, G. C. Transferable GaN Layers Grown on ZnO-Coated Graphene Layers for Optoelectronic Devices. *Science* **2010**, *330*, 655–657.
24. Becerril, H. A.; Mao, J.; Liu, Z.; Stoltenberg, R. M.; Bao, Z.; Chen, Y. Evaluation of Solution-Processed Reduced Graphene Oxide Films as Transparent Conductors. *ACS Nano* **2008**, *2*, 463–470.
25. Tung, V. C.; Kim, J.; Cote, L. J.; Huang, J. Sticky Interconnect for Solution-Processed Tandem Solar Cells. *J. Am. Chem. Soc.* **2011**, *133*, 9262–9265.
26. Zhu, Y.; Sun, Z.; Yan, Z.; Jin, Z.; Tour, J. M. Rational Design of Hybrid Graphene Films for High-Performance Transparent Electrodes. *ACS Nano* **2011**, *5*, 6472–6479.
27. Jeong, C.; Nair, P.; Khan, M.; Lundstrom, M.; Alam, M. A. Prospects for Nanowire-Doped Polycrystalline Graphene Films for Ultratransparent, Highly Conductive Electrodes. *Nano Lett.* **2011**, *11*, 5020–5025.
28. De, S.; King, P. J.; Lyons, P. E.; Khan, U.; Coleman, J. N. Size Effects and the Problem with Percolation in Nanostructured Transparent Conductors. *ACS Nano* **2010**, *4*, 7064–7072.
29. Kaiser, A. B.; Navarro, C. G.; Sundaram, R. S.; Burghard, M.; Kern, K. Electrical Conduction Mechanism in Chemically Derived Graphene Monolayers. *Nano Lett.* **2009**, *9*, 1787–1792.
30. Sundaram, R. S.; Navarro, C. G.; Balasubramanian, K.; Burghard, M.; Kern, K. Electrochemical Modification of Graphene. *Adv. Mater.* **2008**, *20*, 3050–3053.
31. Leem, D. S.; Edwards, A.; Faist, M.; Nelson, J.; Bradley, D. D. C.; de Mello, J. C. Efficient Organic Solar Cells with Solution-Processed Silver Nanowire Electrodes. *Adv. Mater.* **2011**, *23*, 4371–4375.
32. Lee, J. Y.; Connor, S. T.; Cui, Y.; Peumans, P. Solution-Processed Metal Nanowire Mesh Transparent Electrodes. *Nano Lett.* **2008**, *8*, 689–692.
33. Morones, J. R.; Elechiguerra, J. L.; Camacho, A.; Holt, K.; Kouri, J. B.; Ramírez, J. T.; Yacaman, M. J. The Bactericidal Effect of Silver Nanoparticles. *Nanotechnology* **2005**, *16*, 2346–2353.
34. Liu, S.; Zeng, T. H.; Hofmann, M.; Burcombe, E.; Wei, J.; Jiang, R.; Kong, J.; Chen, Y. Antibacterial Activity of Graphite, Graphite Oxide, Graphene Oxide, and Reduced Graphene Oxide: Membrane and Oxidative Stress. *ACS Nano* **2011**, *5*, 6971–6980.
35. Akhavan, O.; Ghaderi, E. Toxicity of Graphene and Graphene Oxide Nanowalls Against Bacteria. *ACS Nano* **2010**, *4*, 5731–5736.
36. Lee, C. Y.; Song, H. G.; Jang, K. S.; Oh, E. J.; Epstein, A. J.; Joo, J. Electromagnetic Interference Shielding Efficiency of Polyaniline Mixtures and Multilayer Films. *Synth. Met.* **1999**, *102*, 1346–1349.
37. Chung, D. D. L. Electromagnetic Interference Shielding Effectiveness of Carbon Materials. *Carbon* **2001**, *39*, 279–285.
38. Liang, J.; Wang, Y.; Huang, Y.; Ma, Y.; Liu, Z.; Cai, J.; Zhang, C.; Gao, H.; Chen, Y. Electromagnetic Interference Shielding of Graphene/Epoxy Composites. *Carbon* **2009**, *47*, 922–925.
39. Xu, H.; Anlage, S. M.; Hu, L.; Gruner, G. Microwave Shielding of Transparent and Conducting Single-Walled Carbon Nanotube Films. *Appl. Phys. Lett.* **2007**, *90*, 183119(1−3).
40. Stankovich, S.; Dikin, D. A.; Dommett, G. H. B.; Kohlhaas, K. M.; Zimney, E. J.; Stach, A.; Piner, R. D.; Nguyen, S. B. T.; Ruoff, R. S. Graphene-Based Composite Materials. *Nature* **2006**, *442*, 282–285.
41. Patil, V.; Malvankar, R. B.; Sastry, M. Role of Particle Size in Individual and Competitive Diffusion of Carboxylic Acid Derivatized Colloidal Gold Particles in Thermally Evaporated Fatty Amine Films. *Langmuir* **1999**, *15*, 8197–8206.